Membrane Composition Determines Pardaxin's Mechanism of Lipid Bilayer Disruption

Kevin J. Hallock,* Dong-Kuk Lee,*†‡ John Omnaas,§ Henry I. Mosberg,†§ and A. Ramamoorthy*†‡
*Department of Chemistry, †Biophysics Research Division, ‡Macromolecular Science and Engineering, §College of Pharmacy, University of Michigan, Ann Arbor, Michigan 48109 USA

ABSTRACT Pardaxin is a membrane-lysing peptide originally isolated from the fish *Pardachirus marmoratus*. The effect of the carboxy-amide of pardaxin (P1a) on bilayers of varying composition was studied using ^{15}N and ^{31}P solid-state NMR of mechanically aligned samples and differential scanning calorimetry (DSC). ^{15}N NMR spectroscopy of [^{15}N-Leu$_{19}$]P1a found that the orientation of the peptide's C-terminal helix depends on membrane composition. It is located on the surface of lipid bilayers composed of 1-palmitoyl-2-oleoyl-phosphatidylcholine (POPC) and is inserted in lipid bilayers composed of 1,2-dimyristoyl-phosphatidylcholine (DMPC). The former suggests a carpet mechanism for bilayer disruption whereas the latter is consistent with a barrel-stave mechanism. The ^{31}P chemical shift NMR spectra showed that the peptide significantly disrupts lipid bilayers composed solely of zwitterionic lipids, particularly bilayers composed of POPC, in agreement with a carpet mechanism. P1a caused the formation of an isotropic phase in 1-palmitoyl-2-oleoyl-phosphatidylethanolamine (POPE) lipid bilayers. This, combined with DSC data that found P1a reduced the fluid lamellar-to-inverted hexagonal phase transition temperature at very low concentrations (1:50,000), is interpreted as the formation of a cubic phase and not micellization of the membrane. Experiments exploring the effect of P1a on lipid bilayers composed of 4:1 POPC:cholesterol, 4:1 POPE:cholesterol, 3:1 POPC:1-palmitoyl-2-oleoyl-phosphatidylglycerol (POPG), and 3:1 POPE:POPG were also conducted, and the presence of anionic lipids or cholesterol was found to reduce the peptide's ability to disrupt bilayers. Considered together, these data demonstrate that the mechanism of P1a is dependent on membrane composition.

INTRODUCTION

Pardaxins are a class of ichthyotoxic peptides isolated from the mucous glands of fish from the genus *Pardachirus* (Lazarovici et al., 1986; Thompson et al., 1986; Adermann et al., 1998). In nature, pardaxins target the gills of fish (Primor, 1985), causing irritation at low concentrations and death at high concentrations (Primor et al., 1980, 1984). Pardaxins also kill bacteria (minimum inhibitory concentrations ranging from 3 to 40 μM), lyse red blood cells (50% hemolysis at 50 μM), and cause leakage from lipid vesicles (Oren and Shai, 1996; Rapaport et al., 1996). Pardaxins are believed to target lipid bilayers, causing leakage of cellular contents (Shai, 1994). As an amphipathic, α-helical peptide, pardaxin's helix-bend-helix structure is similar to many other membrane-active peptides, such as melittin and cecropin (Zagorski et al., 1991). Despite having similar secondary structures, these peptides show different levels of activity and selectivity (Bechinger, 1997; Oren and Shai, 1996). The factors that allow some amphipathic, α-helical peptides to lyse all cells and others to have specificity are not well understood, although it is known that the composition of the membrane is important in determining the selectivity of these peptides (Matsuzaki et al., 1995). Recently, interest in membrane-targeting peptides has increased because of growing bacterial resistance to traditional antibiotics. Antimicrobial peptides offer an alternative method for combating microbes resistant to traditional drugs (Giacometti et al., 2000). Understanding how membrane composition contributes to the selectivity of these peptides will aid in the design of better antimicrobial agents.

Pardaxin was originally isolated from the Red Sea Moses sole, *Pardachirus marmoratus*; it is presumably secreted by the fish to repel predatory fish such as sharks. It is a 33-amino-acid polypeptide, G-F-F-A-L-I-P-K-I-I-S-S-P-L-F-K-T-L-L-S-A-V-G-S-A-L-S-S-S-G-G-Q-E, that has a helix-bend-helix structure in a 1:1 trifluoroethanol and water solution (Zagorski et al., 1991). Residues 7–11 are in a loose right-handed helix whereas residues 14–26 form an α-helix. A hinge centered on Pro$_{13}$ separates the two helices and is essential for the peptide's function (Shai et al., 1990). In this work, the effect of membrane composition on pardaxin's ability to perturb lipid bilayers was studied using NMR and differential scanning calorimetry (DSC).

Solid-state NMR has contributed significantly to the understanding of many different membrane-associated peptides and proteins (Cross and Opella, 1994; Cotten et al., 1997). Typically, ^{15}N NMR of isotopically labeled peptides is used to determine the orientation and structure of peptides in lipid bilayers (Ketchem et al., 1993; Bechinger et al., 1999; Marassi et al., 1997); however, this information describes only the peptide, not its effect on the lipid bilayer. On the other hand, ^{31}P NMR provides information regarding the orientation and dynamics of lipids in peptide-containing bilayers by studying the phosphorus nucleus present in the phospholipid headgroup. The ^{31}P nucleus is 100%

Submitted January 17, 2002, and accepted for publication April 24, 2002.
Address reprint requests to Dr. A. Ramamoorthy, 930 North University, Ann Arbor, MI 48109-1055. Tel.: 734-647-6572; Fax: 734-764-8776; E-mail: ramamoor@umich.edu.

0006-3495/02/08/1004/10 $2.00

naturally abundant and has relatively high sensitivity. Static lipid dispersions are commonly used to study a peptide's effect on membrane structure (Liu et al., 2001; Epand, 1998; Gasset et al., 1988), but ^{31}P powder patterns are broad, and small spectral changes are hard to discern, especially if overlapping powder patterns are present. To avoid this complication, mechanically aligned samples were used throughout this study. In conjunction with ^{31}P NMR, DSC is often used to further characterize a peptide's interaction with lipid bilayers. The effect of a peptide on the fluid lamellar (L_α) to inverted hexagonal (H_{II}) phase transition temperature provides insight into the nature of the peptide-induced curvature strain in the bilayer (Gruner, 1985; Janes, 1996; Matsuzaki et al., 1998). In this work, solid-state NMR and DSC were used to examine the effect of P1a on the structure of bilayers of varying composition, and the results of the experiments reported herein demonstrate that pardaxin's mechanism depends on membrane composition.

MATERIALS AND METHODS

Materials

Fmoc-amino acids were purchased from PerSeptive Biosystems (Foster City, CA) and Advanced ChemTech (Louisville, KY), and isotopically labeled Fmoc-amino acids were from Cambridge Isotope Laboratories (Andover, MA). 1,2-Dipalmitoleoyl-phosphatidylethanolamine (DiPoPE), 1,2-dimyristoyl-phosphatidylcholine (DMPC), 1-palmitoyl-2-oleoyl-phosphatidylcholine (POPC), 1-palmitoyl-2-oleoyl-phosphatidylethanolamine (POPE), and 1-palmitoyl-2-oleoyl-phosphatidylglycerol (POPG) were purchased from Avanti Polar Lipids (Alabaster, AL). Cholesterol was purchased from Sigma (St. Louis, MO), and naphthalene was purchased from Fisher Scientific (Pittsburgh, PA). Chloroform and methanol were purchased from Aldrich Chemical Co. (Milwaukee, WI). All chemicals were used without further analysis or purification.

Synthesis of pardaxin

Pardaxin was synthesized using standard Fmoc-based solid-phase methods with an ABI 431A peptide synthesizer (Applied Biosystems, Foster City, CA). The sequence of the synthesized pardaxin is identical to the peptide isolated from *Pardachirus marmoratus*, G-F-F-A-L-I-P-K-I-I-S-S-P-L-F-K-T-L-L-S-A-V-G-S-A-L-S-S-S-G-G-Q-E (Shai et al., 1988). The carboxy-amide of pardaxin (P1a) was selected because it was easier to synthesize. The addition of an amide at the carboxy terminus increases the peptide's charge by one to a +2 net charge at neutral pH. Although P1a has not been previously researched, many analogs of pardaxin have been studied (Shai et al., 1990, 1991; Rapaport and Shai, 1991; Oren and Shai, 1996). Several analogs had positive charges added at the carboxy terminus with no other modifications and can be used to estimate the membranelysing ability of P1a. The most extensively studied analog had two $[NH(CH_2)_2NH_2]^{2+}$ groups added to its carboxy terminus, giving the peptide a +5 net charge. The +5-charge analog is significantly more hemolytic and antimicrobial than native pardaxin (Oren and Shai, 1996), but it dissipated the diffusion potential of soybean lecithin vesicles at the same rate as native pardaxin (Shai et al., 1990). Therefore, the +5-charge analog is at least as potent as native pardaxin and by extrapolation, we expect P1a to have the same or greater potency than native pardaxin.

Sample preparation

Unless otherwise noted, all samples were prepared using a naphthalene procedure detailed elsewhere (Hallock et al., 2002). Briefly, the membrane components were dissolved in an excess of 2:1 $CHCl_3$:CH_3OH (4 mg of lipids were used for each sample studied with ^{31}P spectroscopy). The lipid-peptide solution was dried with a stream of N_2 gas and then redissolved in 2:1 $CHCl_3$:CH_3OH containing a 1:1 molar ratio of naphthalene to lipid-peptide. The solution was then dried on two thin glass plates (11 mm × 22 mm × 50 μm, Paul Marienfeld, Bad Mergentheim, Germany). To remove the naphthalene and any residual organic solvent, the samples were vacuum dried overnight. The samples were then indirectly hydrated in a sealed container with 93% relative humidity, obtained using a saturated $NH_4H_2PO_4$ solution (Washburn et al., 1926), for 1–2 days at 37°C, after which 28 mol of 4°C water per mol of lipid-peptide were added. The plates were stacked, sealed in plastic (Plastic Bagmart, Marietta, GA), and equilibrated at 4°C for an additional 1–2 days. Two samples used for ^{15}N NMR spectroscopy containing 10 mg of peptide were made using a conventional method because the experiments were done before the development of the naphthalene procedure in our laboratory. The samples were dissolved in 2:1 $CHCl_3$:CH_3OH (no naphthalene was added), dried on glass plates, and vacuum-dried overnight. The samples were then directly hydrated with 25 mol of water per mol of lipid-peptide and allowed to equilibrate in a 93% relative humidity atmosphere for several days. The sample's alignment was confirmed with ^{31}P NMR before conducting ^{15}N NMR experiments. Peptide concentrations are listed as mole percentages throughout the paper.

Solid-state NMR

All experiments were performed at 30°C using a Chemagnetics Infinity 400 MHz solid-state NMR spectrometer operating at a field of 9.4 T with resonance frequencies of 400.14, 161.979, and 40.551 MHz for ^{1}H, ^{31}P, and ^{15}N, respectively. The spectra of mechanically aligned samples were obtained using a home-built double-resonance probe with a four-turn square coil (14 mm × 14 mm × 4 mm) constructed from 2-mm-wide flat-wire with a spacing of 1 mm between turns. The typical 90° pulse length was 3.0 μs for ^{31}P and 3.9 μs for ^{15}N. Unless otherwise noted, all samples were oriented with the bilayer normal parallel to the external magnetic field of the spectrometer. The ^{31}P chemical shift spectra were obtained using a spin-echo sequence (90°-τ-180°-τ, τ = 100 μs) with a proton-decoupling radio frequency (rf) field of 50 kHz, and the second half of the spin-echo was acquired. The ^{31}P chemical shift spectral width was 25 kHz and the recycle delay was 3–5 s. The ^{31}P spectra are referenced relative to 85% H_3PO_4 on thin glass plates (0 ppm). The ^{15}N chemical shift spectra were obtained using a cross-polarization spin-echo sequence with τ delay of 80 μs and with a 67.5-kHz proton-decoupling, and the second half of the spin-echo was acquired. The spectra were referenced to liquid NH_3 (0 ppm) using solid NH_4SO_4 (24.1 ppm). The spectra of dry powder [^{15}N-Leu$_{19}$]P1a were obtained from a sample in a 5-mm MAS rotor using a Chemagnetics/Varian double-resonance MAS probe. Like the aligned samples, a cross-polarization spin-echo sequence was used to acquire the spectra with a contact time of 1 ms with an 86-kHz rf field to decouple protons during acquisition. For the ^{1}H-^{15}N-dipolar-shift-^{15}N-chemical shift experiment (denoted dipolar-shift throughout the paper), the proton decoupling frequency was offset 61 kHz from the water frequency during data acquisition to establish the effective decoupling field at the magic angle (Lee and Ramamoorthy, 1998).

Data processing was accomplished using Spinsight software and IGOR 3.14 (Wavemetrics, Lake Oswego, OR). The parameters of powder patterns were obtained by visually fitting experimental spectra with simulations; the parameters for the best fitting simulation are reported.

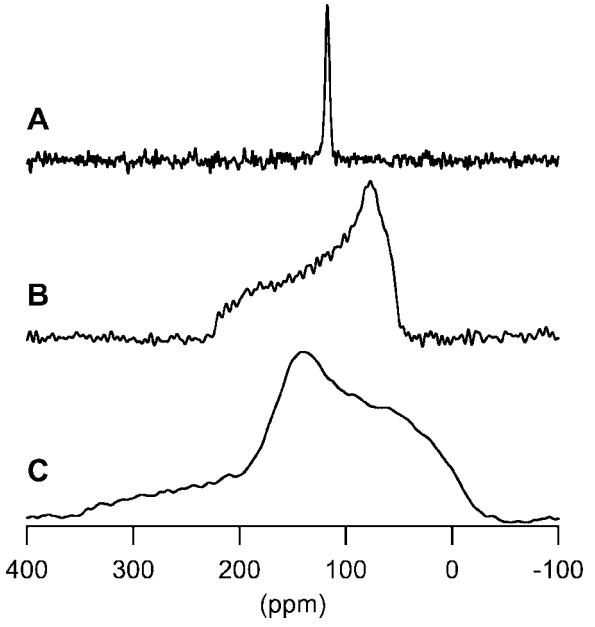

FIGURE 1 Experimental ^{15}N spectra of a dry powder sample of [^{15}N-Leu$_{19}$]P1a. (*A*) CPMAS; (*B*) ^{15}N chemical shift powder pattern; (*C*) ^{1}H-^{15}N-dipolar-shift-^{15}N-chemical shift experiment powder pattern.

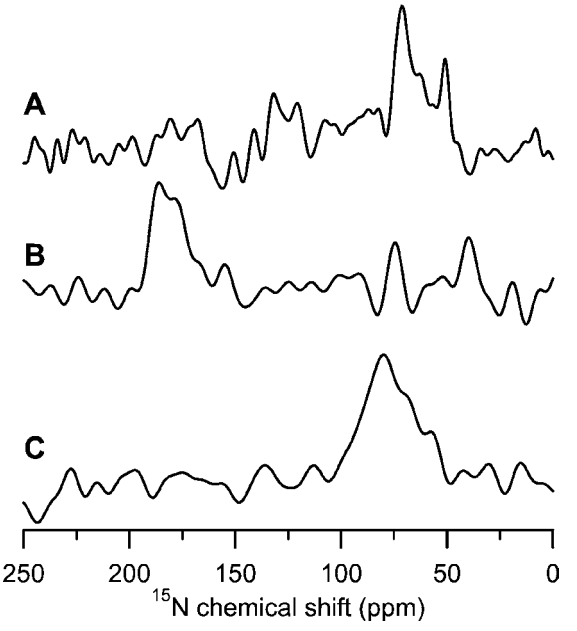

FIGURE 2 Experimental ^{15}N chemical shift spectra of mechanically aligned samples of 2% [^{15}N-Leu$_{19}$]P1a in bilayers composed of POPC (*A*) and DMPC (*B*). Both were aligned with their bilayer normal parallel to the external magnetic field, and these samples were prepared using a conventional method. (*C*) Spectrum of the sample oriented with the bilayer normal perpendicular to the magnetic field for P1a in DMPC.

Differential scanning calorimetry

P1a and DiPoPE were co-dissolved in a 2:1 chloroform:methanol solution (v/v). The solution was dried under a stream of nitrogen and further dried under high vacuum for several hours. Buffer (10 mM Tris/HCl, 100 mM NaCl, 2 mM EDTA, pH 7.4) was added to each sample producing a 10 mg/ml lipid solution, which was vortexed and then degassed. The fluid lamellar phase (L_α) to inverted hexagonal phase (H_{II}) transition temperature of the lipids was measured with a CSC 6100 Nano II differential scanning calorimeter (Calorimetry Sciences Corp., Provo, UT). The scans were processed using the software provided by the manufacturer. The heating rate of all experiments was 0.25°C/min.

RESULTS

^{15}N NMR of P1a

[^{15}N-Leu$_{19}$]P1a was synthesized to determine the orientation of the peptide's C-terminal amphipathic helix in lipid bilayers using mechanically aligned samples. Knowledge of the magnitude and orientation of the chemical shift tensor in the molecular frame is necessary to interpret ^{15}N chemical shift spectra of aligned samples, so these parameters were determined from a dry powder sample of [^{15}N-Leu$_{19}$]P1a. First, cross-polarization and magic-angle sample spinning (CPMAS) was used to determine the isotropic chemical shift, σ_{iso} = 117.4 ppm (Fig. 1 *A*). The isotropic chemical shift corresponds to a leucine residue contained within an α-helix (Shoji et al., 1987), implying the parameters found in the powder are relevant to the expected secondary structure of P1a in lipid bilayers based on solution NMR studies (Zagorski et al., 1991). From the chemical shift powder pattern (Fig. 1 *B*), the magnitudes of the ^{15}N chemical shift tensor were found to be σ_{11} = 52 ppm, σ_{22} = 77 ppm, and σ_{33} = 224 ppm with errors estimated to be ±2 ppm. The orientation of the chemical shift tensor in the molecular frame was determined using a one-dimensional dipolar-shift experiment (Lee and Ramamoorthy, 1998). From this experiment, a dipolar-shift powder pattern of P1a was obtained (Fig. 1 *C*); the angle between σ_{33} and the N-H bond was found to be 20 ± 5°, whereas the angle between σ_{11} and the plane perpendicular to the N-H bond was determined to be 30 ± 15°. (The best fitting simulation of the one-dimensional dipolar shift spectrum was obtained using a dipolar coupling of 9.7 kHz, which corresponds to an N-H bond length of 1.08 Å.)

With the orientation of the chemical shift tensor with respect to the N-H bond determined from the dry powder, an aligned spectrum easily distinguishes between a transmembrane and surface orientation of the peptide. Because the N-H bond is approximately collinear with the helical axis, an inserted orientation would yield a spectrum with a peak at a chemical shift near σ_{33} (~200 ppm) and a surface orientation would produce a peak close to σ_{11} and σ_{22} (~60 ppm). To determine the orientation of the C-terminal helix of P1a, several ^{15}N NMR experiments were performed on samples of 2% [^{15}N-Leu$_{19}$]P1a in POPC bilayers aligned on glass plates. The best spectrum obtained from these experiments is shown in Fig. 2 *A*. There are two peaks, one at 70 ppm and the other at 50 ppm. The latter peak is likely caused by natural abundance background whereas the peak

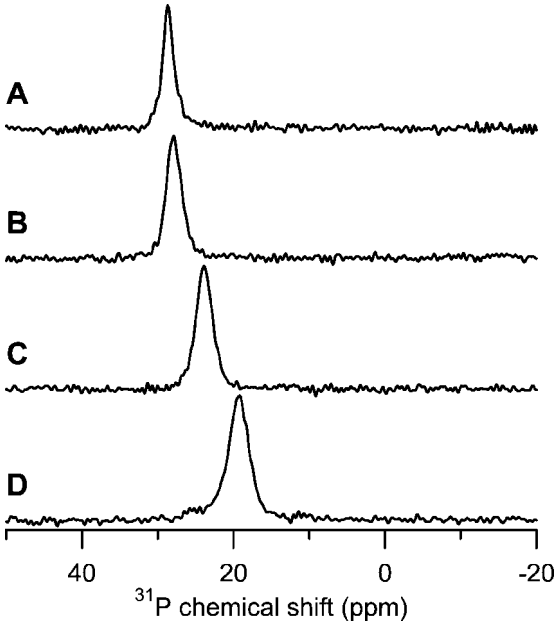

FIGURE 3 Experimental ^{31}P chemical shift spectra of mechanically aligned samples of POPC and specific mole percentages of P1a. (*A*) 0% P1a; (*B*) 1% P1a; (*C*) 3% P1a; (*D*) 5% P1a.

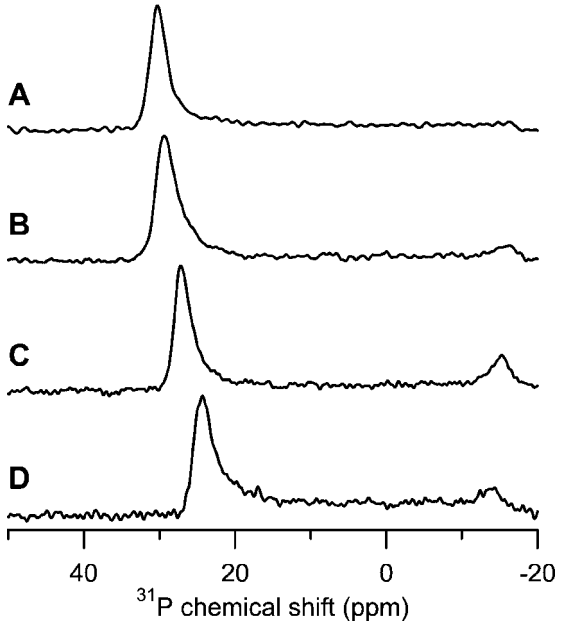

FIGURE 4 Experimental ^{31}P chemical shift spectra of mechanically aligned samples of DMPC and specific mole percentages of P1a. (*A*) 0% P1a; (*B*) 1% P1a; (*C*) 3% P1a; (*D*) 5% P1a.

at 70 ppm suggests that the amphipathic helix is lying on the surface of the bilayer. However, the signal-to-noise ratio is poor considering the spectrum consists of 65,000 transients obtained from a sample containing 10.8 mg of peptide. A similar experiment was conducted with 11.1 mg of P1a in DMPC, and the resulting spectrum is shown in Fig. 2 *B*. This spectrum, consisting of only 13,000 transients, has a peak near 180 ppm indicating the amphipathic helix is inserted into the DMPC bilayer. This sample was rotated 90°, positioning the bilayer normal perpendicular to the magnetic field, and a ^{15}N chemical shift spectrum was obtained. Fig. 2 *C* shows this spectrum, consisting of a single peak at 80 ppm. These two peaks are not at the edges of the rigid powder pattern (Fig. 1 *B*), which implies that P1a is undergoing motion on a timescale fast enough to partially average the chemical shift anisotropy (CSA) and/or the peptide's helix is tilted with respect to the bilayer normal. These ^{15}N spectra demonstrate that the C-terminal helix of P1a is located on the surface of POPC bilayers and inserted in DMPC bilayers.

^{31}P NMR of P1a in zwitterionic lipid bilayers

Changes in the lipid headgroup region caused by increasing concentrations of P1a in POPC (Fig. 3), DMPC (Fig. 4), and POPE (Fig. 5) were monitored using ^{31}P NMR spectroscopy. In Fig. 3, the ^{31}P chemical shift spectra of mechanically aligned POPC bilayers containing 0–5% P1a are shown. The spectrum of POPC (Fig. 3 *A*) yielded a single, intense peak at 28.7 ppm indicative of a well-aligned sample. Each concentration of peptide tested had a single intense peak; however, the peak position shifted to lower frequency with increasing peptide concentration: 27.9 ppm at 1% P1a (Fig. 3 *B*), 23.9 ppm at 3% P1a (Fig. 3 *C*), and 19.2 ppm at 5% P1a (Fig. 3 *D*). By acquiring spectra with the bilayer normal at 30°, 50°, and 90° with respect to the

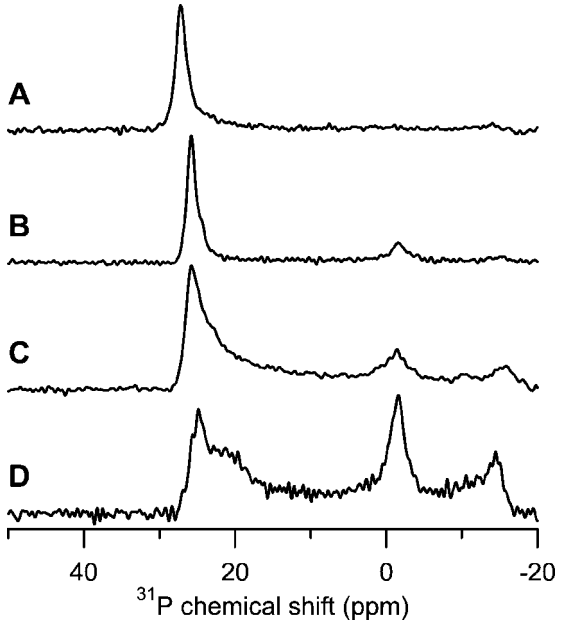

FIGURE 5 Experimental ^{31}P chemical shift spectra of mechanically aligned samples of POPE and specific mole percentages of P1a. (*A*) 0% P1a; (*B*) 1% P1a; (*C*) 3% P1a; (*D*) 5% P1a.

magnetic field (data not shown), motional narrowing of the CSA was identified as the cause of this frequency shift. Increasing concentrations of P1a similarly narrowed the ^{31}P CSA span of DMPC (Fig. 4): 30.1 ppm at 0% P1a, 29.4 ppm at 1% P1a, 27.2 ppm at 3% P1a, and 24.3 ppm at 5% P1a (Fig. 4, *A–D*, respectively), although not to the extent observed in POPC bilayers. To understand the relative significance of these changes, the breadth of the ^{31}P CSA of pure POPC and pure DMPC were characterized and found to be 46 ppm and 50 ppm, respectively (data not shown). Thus, the ^{31}P CSA span of POPC reduced by 31% from 0 to 5% P1a concentration, whereas the ^{31}P CSA span of DMPC decreased only by 17% suggesting that P1a perturbs the lipids in POPC more than in DMPC.

The simplicity of the ^{31}P spectra of phosphatidylcholine lipids contrasts with the spectra of POPE bilayers containing P1a (Fig. 5). The ^{31}P chemical shift spectrum of POPE shown in Fig. 5 *A* demonstrates that the POPE bilayers were well aligned in the absence of peptide with a single peak at 27.2 ppm. Unlike POPC, a peak near 27 ppm was observed in all of the spectra. In addition, two spectral features developed with increasing peptide concentration. One feature was a broad component spanning from the aligned peak to ~−16 ppm that increased in intensity with peptide concentration. Another was the appearance of an isotropic peak at −1.6 ppm, initially evident at 1% P1a with a concentration-dependent increase in intensity (Fig. 5, *B–D*). An isotropic peak can be indicative of the formation of micelles or cubic lipid phases. The latter is more likely when considered with the DSC data discussed later.

^{31}P NMR of P1a in cholesterol-containing lipid bilayers

Cholesterol is commonly found in mammalian cell membranes and inhibits some membrane-lysing peptides (Tytler et al., 1995; Matsuzaki et al., 1995; Benachir et al., 1997; Hincha and Crowe, 1996; Feigin et al., 1995). Although there is no direct evidence that pardaxin is inhibited by cholesterol, it is known that pardaxin is antimicrobial at lower concentrations than it is hemolytic (Oren and Shai, 1996). To determine whether P1a exhibits similar behavior, aligned bilayers composed of 4:1 POPC:cholesterol and 4:1 POPE:cholesterol were studied. ^{31}P chemical shift spectra of 4:1 POPC:cholesterol bilayers containing 0–5% P1a are shown in Fig. 6. The spectrum of 4:1 POPC:cholesterol (Fig. 6 *A*) revealed a single peak at 28.4 ppm, consistent with a well-aligned bilayer. At 1% P1a (Fig. 6 *B*), the peak shifted to 26.8 ppm and broadened. With 3% P1a present (Figs. 6 *C*), two peaks were present; the highest intensity peak was at 26.3 ppm and another near 21.3 ppm, suggesting the formation of two domains within the sample. When the concentration of P1a was increased to 5% (Fig. 6 *D*), the 26.3 ppm peak shifted to 25.6 ppm, whereas the low-intensity peak broadened and moved to 15.5 ppm. In bilayers composed of 4:1 POPE:cholesterol (Fig. 7), higher peptide concentrations led to an increasingly intense broad component similar to that observed in bilayers composed of POPE (Fig. 5), but the pronounced isotropic peak observed in the sample of POPE containing 5% P1a (Fig. 5 *D*) was not present at 5% peptide in 4:1 POPE:cholesterol (Fig. 7

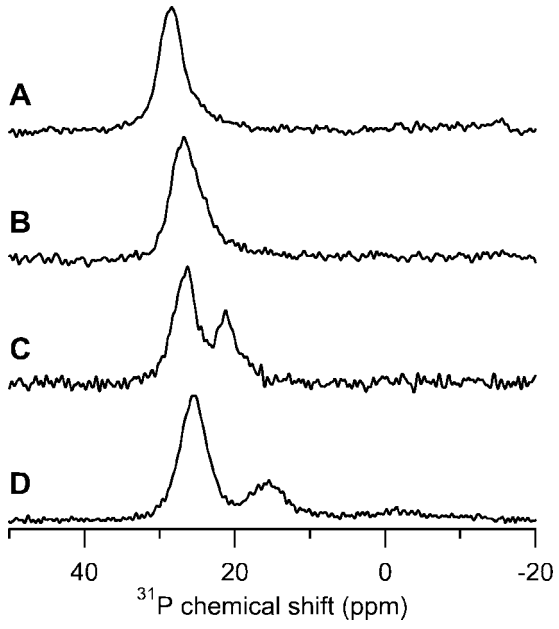

FIGURE 6 Experimental ^{31}P chemical shift spectra of mechanically aligned samples of 4:1 POPC:cholesterol and specific mole percentages of P1a. (*A*) 0% P1a; (*B*) 1% P1a; (*C*) 3% P1a; (*D*) 5% P1a.

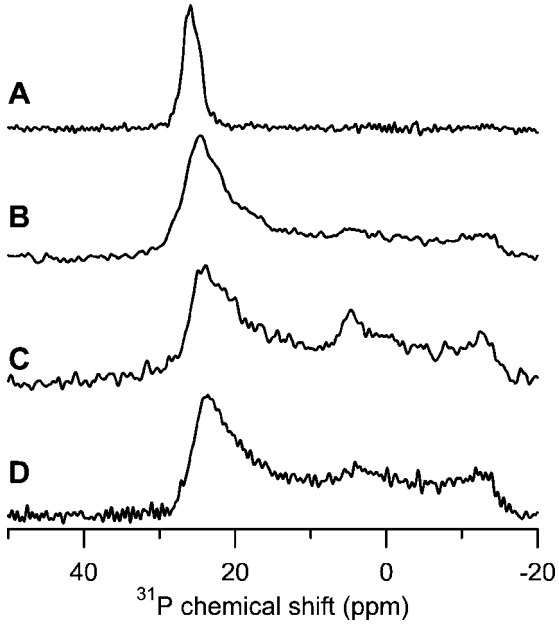

FIGURE 7 Experimental ^{31}P chemical shift spectra of mechanically aligned samples of 4:1 POPE:cholesterol and specific mole percentages of P1a. (*A*) 0% P1a; (*B*) 1% P1a; (iC) 3% P1a; (*D*) 5% P1a.

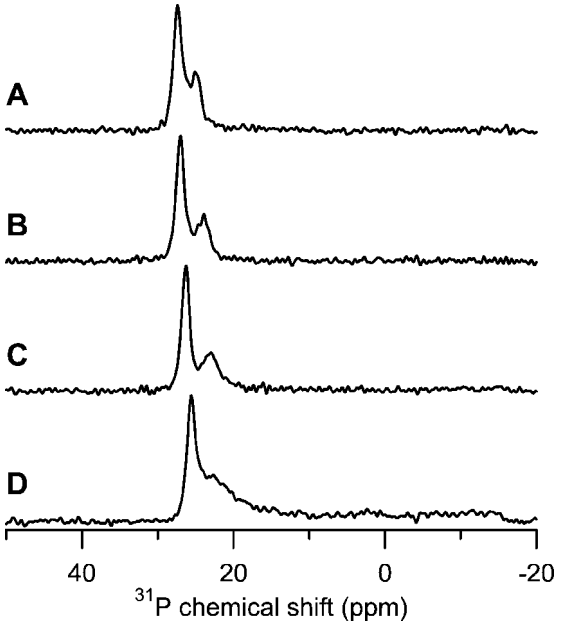

FIGURE 8 Experimental ^{31}P chemical shift spectra of mechanically aligned samples of 3:1 POPC:POPG and specific mole percentages of P1a. (*A*) 0% P1a; (*B*) 1% P1a; (*C*) 3% P1a; (*D*) 5% P1a.

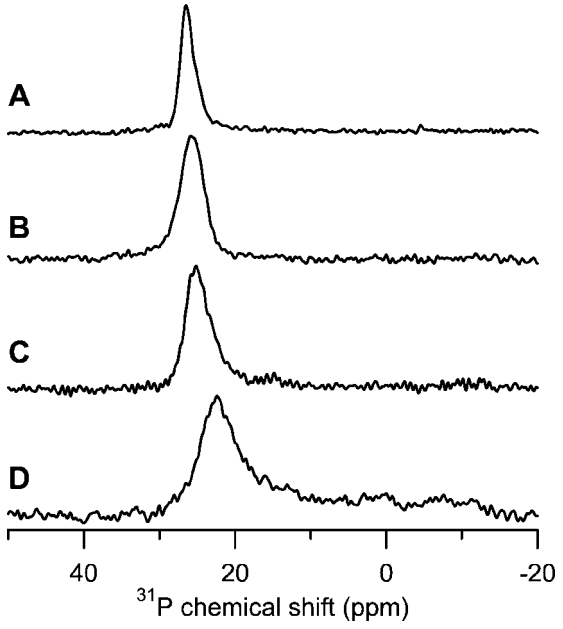

FIGURE 9 Experimental ^{31}P chemical shift spectra of mechanically aligned samples of 3:1 POPE:POPG and specific mole percentages of P1a. (*A*) 0% P1a; (*B*) 1% P1a; (*C*) 3% P1a; (*D*) 5% P1a.

D). A small peak is present in the 3% and 5% P1a sample near 4.7 ppm (Fig. 7, *C* and *D*) but is greatly reduced compared with the peak at −1.6 ppm observed in the POPE samples (Fig. 5, *C* and D*)*. These spectra suggest cholesterol inhibits the ability of P1a to disrupt the headgroups of lipid bilayers.

^{31}P NMR of P1a in POPG-containing lipid bilayers

Anionic lipids are important components of many cellular membranes, particularly bacterial membranes (Hincha and Crowe, 1996). The presence of anionic lipids in bacterial membranes is considered an important selectivity filter for cationic antimicrobial peptides. The spectra shown in Figs. 8 and 9 demonstrate that POPG alters the ability of P1a to disrupt lipid bilayers. Figs. 8 and 9 show the ^{31}P chemical shift spectra of lipid bilayers containing POPG combined with POPC or POPE, respectively. In bilayers composed of 3:1 POPC:POPG without P1a, the ^{31}P chemical shift spectrum exhibited two peaks, one at 27.4 and the other at 25.2 ppm (Fig. 8 *A*). The relative area of these peaks is 3:2, suggesting that the signal is not from individual lipids, but from POPG-rich and POPG-poor domains. Because the sample contained only 25% POPG, the less intense (25.2 ppm) peak was assigned to the POPG-rich domain. The peak near 27.4 ppm remained relatively unperturbed as the peptide concentration increased, whereas the lower-frequency peak shifted a little and broadened significantly (Fig. 8, *B–D*). This indicates that P1a preferentially interacts with the POPG-rich domain. Fig. 9 shows the ^{31}P chemical shift spectra of aligned bilayers composed of 3:1 POPE:POPG and different concentrations of P1a. Unlike bilayers composed of 3:1 POPC:POPG (Fig. 8 *A*), only one peak was observed with 3:1 POPE:POPG (Fig. 9 *A*), suggesting that separate domains do not form in these bilayers. The inclusion of P1a broadened and shifted this peak with increasing concentration. At 1% P1a, the 26.3 ppm peak had a full-width at half-maximum (FWHM) of 2 ppm (Fig. 9 *B*). With 3% P1a, the peak shifted to 25.2 ppm and a FWHM of 3.7 ppm. By 5% P1a, the peak was located at 22.3 ppm with a FWHM of 5.6 ppm, and a low-intensity broad component was also present (Fig. 9 *D*). Noticeably absent from the spectrum of 5% P1a in 3:1 POPE:POPG was the intense isotropic signal found at the same peptide concentration in POPE bilayers (Fig. 5 *D*). These data suggest that the presence of POPG significantly changes the peptide's interaction with the bilayer, despite the peptide's low net positive charge.

DSC of P1a in DiPoPE

DSC was used to study the effect of P1a on membrane curvature by monitoring the peptide's influence on the L_α to H_{II} phase transition temperature (T_H) of pure DiPoPE. DSC heating thermograms are shown in Fig. 10; Fig. 10 *A* shows that DiPoPE exhibits a T_H of 42°C, as expected. At a low peptide-to-lipid ratio of 1:50,000 (Fig. 1 *B*), T_H was decreased to 39.1°C. By increasing the peptide concentration to a peptide-to-lipid ratio of 1:17,000 (Fig. 10 *C*), T_H further reduced to 38.3°C. No distinct phase transition was ob-

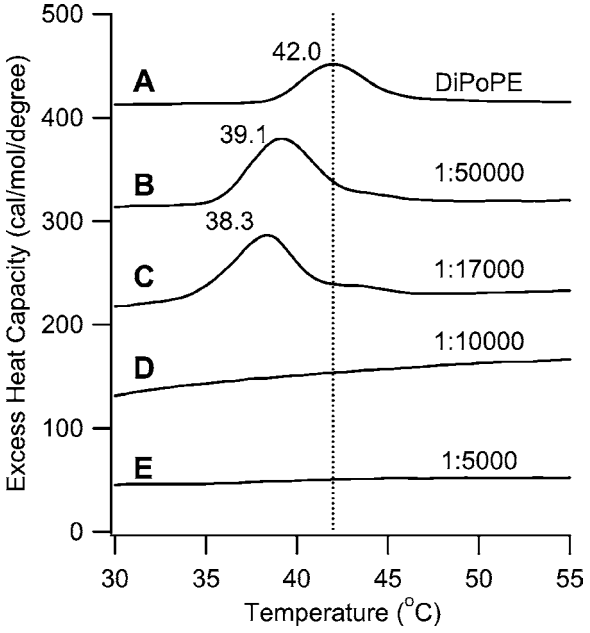

FIGURE 10 DSC heating thermograms of pardaxin in DiPoPE are shown at the listed peptide-to-lipid ratios. The scan rate was +0.25°C/min. The position of the scans along the vertical axis is arbitrary as this axis is included for scaling purposes. (*A*) DiPoPE without peptide; (*B*) 1:50,000; (*C*) 1:17,000; (*D*) 1:10,000; (*E*) 1:5,000.

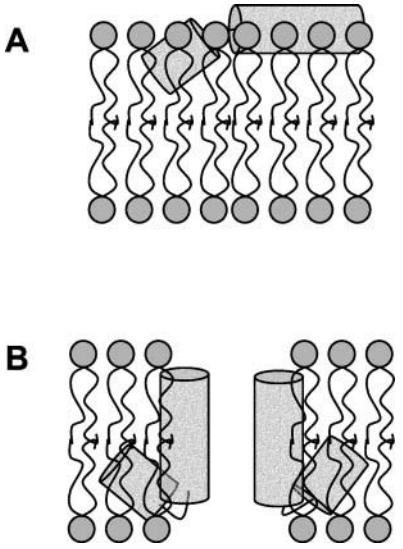

FIGURE 11 Model of P1a in lipid bilayers based on the ^{15}N spectra shown in Fig. 2. The longer helical tube represents the amphipathic (C-terminal) helix and the hydrophobic (N-terminal) helix is the shorter helical tube. (*A*) P1a in POPC; the amphipathic helix is on the surface of the bilayer. (*B*) P1a in DMPC; the peptides form a barrel-stave channel with the amphipathic helix inserted into the bilayer with the hydrophilic faces presumably lining the pore. No information is currently known about the relative orientation of the hydrophobic helix with respect to the amphipathic helix. The hydrophobic helix is included in the figure for the sake of completeness.

served at higher peptide concentrations (Fig. 10, *D* and *E*). To the best of our knowledge, no peptide has been reported that influences T_H at such low concentrations. At the miniscule peptide concentrations used, P1a is unlikely to be able to influence the bulk behavior of the lipids and probably adopts a catalytic role in the phase transition, as will be discussed later.

DISCUSSION

Lytic peptides, such as pardaxin and melittin, exist throughout nature; these peptides often lyse a wide variety of cellular membranes, including those of bacterial and mammalian cells. The composition of membranes is known to modulate the effectiveness of several of these peptides, but this study reports the first evidence that pardaxin's ability to disrupt membranes is dependent on membrane composition. In this work, we probed the effect of membrane composition on the ability of the carboxy-amide of pardaxin (P1a) to disrupt model membranes. The composition of model membranes was varied to probe the influence of anionic lipids and cholesterol on the ability of P1a to cause membrane disruption. These two components were selected because their presence differentiates mammalian membranes, which contain cholesterol, from bacterial membranes, which contain 20–25% anionic lipids.

All of the data presented here suggest that the mechanism of P1a is dependent on the bilayer's composition. From ^{15}N NMR spectroscopy, [^{15}N-Leu$_{19}$]P1a was found to have different orientations in POPC and DMPC bilayers, as depicted in Fig. 11. In POPC, the amphipathic helix is approximately parallel to the bilayer surface (Fig. 11 *A*), whereas in DMPC the peptide is inserted, probably forming a barrel-stave channel as illustrated in Fig. 11 *B* (Rapaport and Shai, 1992). Further support for a barrel-stave channel in DMPC bilayers is found when comparing the linewidths of the peaks observed from the parallel (Fig. 2 *B*) and perpendicular (Fig. 2 *C*) sample orientations. In a barrel-stave channel, the peptides comprising the channel would have identical orientations with respect to the magnetic field in the parallel sample alignment, but the orientations would be different in the perpendicular orientation, causing the observed peak to be broader. Why the peptide is located on the surface of POPC bilayers and inserted in DMPC bilayers is unknown. One possibility is hydrophobic mismatch between the peptide and the bilayer. Hydrophobic mismatch is important in determining a peptide's orientation in lipid bilayers (Harzer and Bechinger, 2000), but there is only a 3-Å difference between the hydrophobic thickness of DMPC and POPC, and the effect of such a small difference is unknown (Marsh, 1990).

As noted previously, the ^{15}N spectra observed from P1a in DMPC bilayers (Fig. 2, *B* and *C*) indicate that the peptide is tilted with respect to the bilayer normal and/or undergoing motion. If tilt is assumed to be the sole cause, the

C-terminal helix of the peptide would need to be at a 30° angle with respect to the bilayer normal. However, the data acquired using ^{31}P NMR spectroscopy suggest that the lipids are undergoing additional motion with increasing peptide concentration (Figs. 3 and 4). Because the uniaxial rotation of the lipids is fast on the NMR timescale, the motional averaging of the ^{31}P CSA is likely a wobbling and/or reorientation of the headgroup leading to a different average conformation (Thayer and Kohler, 1981). In DMPC bilayers, P1a disrupts the lipids and narrows the ^{31}P CSA (Fig. 4); this effect is even more pronounced in POPC bilayers (Fig. 3). Considering the ^{15}N spectra of mechanically aligned bilayers in this context, we believe that coupled motions between the lipids and the peptide contribute to the observed ^{15}N spectra of P1a in DMPC bilayers. This is further supported by the poor signal-to-noise ratio of the ^{15}N chemical shift spectrum of P1a in POPC sample (Fig. 2 *A*), which is probably due to motion of the peptide on the surface of the bilayer. Extensive motions that reduce cross-polarization efficiency could cause the poor signal-to-noise ratio observed in the spectrum of the isotopically labeled peptide. The general destabilization of POPC bilayers suggests a carpet mechanism for cell lysis, in which the peptide disrupts the bilayer to a large extent, allowing leakage of cellular contents. Even though the peptide causes similar motion in DMPC bilayers (Fig. 4), its effect is significantly smaller than was observed with POPC. The ^{15}N data establishes that P1a inserts into DMPC bilayers consistent with a barrel-stave mechanism in these bilayers.

P1a exhibited a different effect on POPE than on the bilayers composed of phosphatidylcholine lipids, establishing that differences in the acyl chains between POPC and DMPC bilayers is not the only factor that can affect the peptide's activity. The peptide caused the formation of an isotropic peak in a concentration-dependent manner in POPE (Fig. 5). Although this peak could be caused by either micellization of the bilayer or the formation of a cubic phase, the DSC data suggest the latter is more likely. The DSC data showed that P1a reduced the phase transition temperature of DiPoPE beginning at concentrations of 1:50,000. At these low concentrations, P1a is unable to influence all of the bulk lipids. Probably P1a stabilizes an intermediate phase between the L_α and H_{II} phases; these intermediates have been postulated to be similar to a cubic phase (Siegel, 1999). Whether micellization or cubic phase formation is responsible for the isotropic peak, P1a clearly operates via a different mechanism in POPE bilayers than in those composed of phosphatidylcholine lipids. An unusual characteristic of this peak is that it is only observed in bilayers composed solely of phosphatidylethanolamine lipids; the addition of cholesterol or anionic lipids prevents its formation.

Inhibition of membrane-lysing peptides by cholesterol has been reported, but the source of the inhibition is not well understood (Tytler et al., 1995; Matsuzaki et al., 1995; Benachir et al., 1997; Hincha and Crowe, 1996; Feigin et al., 1995). The inclusion of cholesterol in lipid bilayers reduces the ability of P1a to disrupt the lipid bilayers tested. In 4:1 POPC:cholesterol bilayers (Fig. 6), a single peak is observed in the absence of peptide (Fig. 6 *A*), which divides into two peaks with increasing peptide concentration (Fig. 6, *C* and *D*). Because POPC is the only source for phosphorus signal in this sample, the peaks must originate from lipids in different domains. The domain that is the source of the peak near 30 ppm remained unperturbed with increasing concentrations of P1a, whereas the other shifts to lower frequency. The concentration-dependent shift of the lower-frequency peak is similar to the frequency shift observed in the ^{31}P spectra of POPC bilayers (Fig. 3), suggesting this peak originated from a cholesterol-poor domain. Assuming this, the peak near 30 ppm originates from a cholesterol-rich domain unperturbed by the peptide, demonstrating that cholesterol inhibits the function of P1a. Similar results were found with POPE-containing bilayers. The presence of cholesterol in 4:1 POPE:cholesterol bilayers prevented the formation of the peptide-induced isotropic phase that was observed in POPE bilayers. Comparing 5% P1a in 4:1 POPE:cholesterol (Fig. 9 *D*) with the same peptide concentration in POPE (Fig. 5 *D*), no isotropic peak was observed in the cholesterol-containing bilayers.

Like cholesterol, anionic lipids suppress the ability of P1a to disrupt lipid bilayers. The ^{31}P chemical shift spectrum of 3:1 POPC:POPG has two peaks, one at 27.4 and the other at 25.2 ppm (Fig. 8 *A*) with the less-intense 25.2-ppm peak assigned to the POPG-rich domain and the 27.4 ppm peak to the POPG-poor domain. With increasing peptide concentration, the peak from the POPG-rich region is broadened until there is no longer a distinct second peak at 5% P1a (Fig. 8 *D*), indicating P1a has a preferential interaction with anionic phospholipids. As in the case of 4:1 POPC:cholesterol bilayers, only one domain was perturbed by the peptide, leaving many lipids unaffected. Lipids within the perturbed domain are undergoing significant additional motion based on the ^{31}P NMR spectra, which is consistent with a carpet mechanism. Inhibition of P1a by POPG was observed in bilayers composed of 3:1 POPE:POPG (Fig. 9). The presence of POPG prevented the formation of an isotropic component in bilayers containing POPE (compare Fig. 5 *D* with Fig. 9 *D*). These results are surprising because there is no evidence that pardaxin's ability to permeate anionic vesicles is different from zwitterionic vesicles (Shai, 1994). However, P1a has a larger net charge than pardaxin because it is amidated, which might lead to a stronger interaction between the carboxy terminus and the negatively charged POPG headgroup than the native peptide.

In summary, the ^{31}P data discussed here demonstrate that P1a significantly disrupts bilayers composed of only zwitterionic lipids, although the extent of the disruption is modulated by the nature of the lipid's acyl chains. The addition of either cholesterol or POPG to the model membrane

reduces the ability of P1a to disrupt the bilayer. In 4:1 POPC:cholesterol and 3:1 POPC:POPG bilayers, the disruption was localized to cholesterol-poor or POPG-rich domains, but these domains were still disrupted. The presence of localized disruption is consistent with the carpet mechanism; only a portion of a cellular membrane in vivo needs to be weakened to allow the unregulated passage of ions. In 4:1 POPE:cholestrol and 3:1 POPE:POPG bilayers, the presence of cholesterol or POPG completely prevented the formation of an isotropic peak. Bilayer disruption is not a prerequisite for a barrel-stave mechanism, but peptides forming a barrel-stave pore should have a defined orientation that can be easily observed using an isotopically labeled peptide. However, attempts to acquire ^{15}N spectra of P1a in POPE bilayers have so far failed, most likely due to motion of the peptide that interferes with the Hartmann-Hahn condition during cross-polarization experiments. Even without additional ^{15}N data, the data presented here demonstrate that the ability of P1a to disrupt lipid bilayers depends on the composition of the bilayer. Previously, others suggested that pardaxin operates by more than one mechanism (Lazarovici et al., 1986), but they reported pardaxin had a concentration-dependent mechanism. This work expands the earlier observation to include membrane composition. The inhibition of P1a by cholesterol is not surprising because pardaxin does not lyse mammalian cells to the extent it lyses bacterial membranes (Oren and Shai, 1996); however, the effect of POPG was surprising as discussed above, but this could be caused by the increased cationic charge of P1a.

These data suggest that the membrane-lysing mechanisms of P1a are complex. Using lipid bilayers mimicking mammalian and bacterial membranes, P1a was found to have a composition-dependent mechanism of bilayer disruption. It is unlikely that P1a is the only membrane-lysing peptide operating by more than one mechanism. Multimechanism peptides would have an evolutionary advantage, particularly venoms like melittin and mastoparan. Understanding what determines which mechanism is employed might allow peptidic antibiotics to be developed that target specific membranes, such as cancer cells, while leaving other membranes unaffected.

We thank Jose Santos and Katherine Henzler Wildman for useful discussions.

This research was partly supported by the research funds from the National Science Foundation (Career Development Award to A.R.). K.J.H. was supported by the National Institutes of Health-Michigan Molecular Biophysics Training Program (GM08270).

REFERENCES

Adermann, K., M. Raida, Y. Paul, S. Aburaya, E. Blochshilderman, P. Lazarovici, J. Hochman, and H. Wellhoner. 1998. Isolation, characterization and synthesis of a novel Pardaxin isoform. 435:173–177.

Bechinger, B. 1997. Structure and functions of channel-forming peptides: magainins, cecropins, melittin and alamethicin. *J. Membr. Biol.* 156: 197–211.

Bechinger, B., R. Kinder, M. Helmle, T. C. B. Vogt, U. Harzer, and S. Schinzel. 1999. Peptide structural analysis by solid-state NMR spectroscopy. *Biopolymers.* 51:174–190.

Benachir, T., M. Monette, J. Grenier, and M. Lafleur. 1997. Melittin-induced leakage from phosphatidylcholine vesicles is modulated by cholesterol: a property used for membrane targeting. *Eur. Biophys. J. Biophys. Lett.* 25:201–210.

Cotten, M., V. G. Soghomonian, W. Hu, and T. A. Cross. 1997. High resolution and high fields in biological solid state NMR. *Solid State Nuclear Magn. Reson.* 9:77–80.

Cross, T. A., and S. J. Opella. 1994. Solid-state NMR structural studies of peptides and proteins in membranes. *Curr. Opin. Struct. Biol.* 4:574–581.

Epand, R. M. 1998. Lipid polymorphism and protein-lipid interactions. *Biochim. Biophys. Acta.* 1376:353–368.

Feigin, A. M., J. H. Teeter, and J. G. Brand. 1995. The influence of sterols on the sensitivity of lipid bilayers to melittin. *Biochem. Biophys. Res. Commun.* 211:312–317.

Gasset, M., J. A. Killian, H. Tournois, and B. de Kruijff. 1988. Influence of cholesterol on gramicidin-induced H_{II} phase formation in phosphatidylcholine model membranes. *Biochim. Biophys. Acta.* 939:79–88.

Giacometti, A., O. Cirioni, R. Ghiselli, L. Goffi, F. Mocchegiani, A. Riva, G. Scalise, and V. Saba. 2000. Efficacy of polycationic peptides in preventing vascular graft infection due to *Staphylococcus epidermidis*. *J. Antimicrob. Chemother.* 46:751–756.

Gruner, S. M. 1985. Intrinsic curvature hypothesis for biomembrane lipid composition: a role for nonbilayer lipids. *Proc. Natl. Acad. Sci. U.S.A.* 82:3665–3669.

Hallock, K. J., K. A. Henzler Wildman, D. K. Lee, and A. Ramamoorthy. 2002. An innovative procedure using a sublimable solid to align lipid bilayers for solid-state NMR studies. *Biophys. J.* 82:2499-2503.

Harzer, U., and B. Bechinger. 2000. Alignment of lysine-anchored membrane peptides under conditions of hydrophobic mismatch: a CD, N-15 and P-31 solid-state NMR spectroscopy investigation. *Biochemistry.* 39:13106–13114.

Hincha, D. K., and J. H. Crowe. 1996. The lytic activity of the bee venom peptide melittin is strongly reduced by the presence of negatively charged phospholipids or chloroplast galactolipids in the membranes of phosphatidylcholine large unilamellar vesicles. *Biochim. Biophys. Acta. Biomembr.* 1284:162–170.

Janes, N. 1996. Curvature stress and polymorphism in membranes. *Chem. Phys. Lipids.* 81:133–150.

Ketchem, R. R., W. Hu, and T. A. Cross. 1993. High-resolution conformation of gramicidin A in a lipid bilayer by solid-state NMR. *Science.* 261:1457–1460.

Lazarovici, P., N. Primor, and L. M. Loew. 1986. Purification and pore-forming activity of two hydrophobic polypeptides from the secretion of the Red Sea Moses sole (*Pardachirus marmoratus*). *J. Biol. Chem.* 261:16704–16713.

Lee, D. K., and A. Ramamoorthy. 1998. A simple one-dimensional solid-state NMR method to characterize the nuclear spin interaction tensors associated with the peptide bond. *J. Magn. Res.* 133:204–206.

Liu, F., R. Lewis, R. S. Hodges, and R. N. McElhaney. 2001. A differential scanning calorimetric and P-31 NMR spectroscopic study of the effect of transmembrane alpha-helical peptides on the lamellar-reversed hexagonal phase transition of phosphatidylethanolamine model membranes. *Biochemistry.* 40:760–768.

Marassi, F. M., A. Ramamoorthy, and S. J. Opella. 1997. Complete resolution of the solid-state NMR spectrum of a uniformly N-15-labeled membrane protein in phospholipid bilayers. *Proc. Natl. Acad. Sci. U.S.A.* 94:8551–8556.

Marsh, D. 1990. CRC Handbook of Lipid Bilayers. CRC Press, Boca Raton, FL.

Matsuzaki, K., K. Sugishita, N. Fujii, and K. Miyajima. 1995. Molecular basis for membrane selectivity of an antimicrobial peptide, magainin 2. *Biochemistry.* 34:3423–3429.

Matsuzaki, K., K. Sugishita, N. Ishibe, M. Ueha, S. Nakata, K. Miyajima, and R. M. Epand. 1998. Relationship of membrane curvature to the formation of pores by magainin 2. *Biochemistry.* 37:11856–11863.

Oren, Z., and Y. Shai. 1996. A class of highly potent antibacterial peptides derived from pardaxin, a pore-forming peptide isolated from Moses sole fish *Pardachirus marmoratus*. *Eur. J. Biochem.* 237:303–310.

Primor, N. 1985. Pharyngeal cavity and the gills are the target organ for the repellent action of pardaxin in shark. *Experientia.* 41:693–5.

Primor, N., I. Sabnay, V. Lavie, and E. Zlotkin. 1980. Toxicity to fish, effect on gill ATPase and gill ultrastructural-changes induced by pardachirus secretion and its derived toxin pardaxin. *J. Exp. Zool.* 211: 33–43.

Primor, N., J. A. Zadunaisky, H. V. Murdaugh, Jr., J. L. Boyer, and J. N. Forrest, Jr. 1984. Pardaxin increases solute permeability of gills and rectal gland in the dogfish shark (*Squalus acanthias*). *Comp. Biochem. Physiol. C.* 78:483–490.

Rapaport, D., R. Peled, S. Nir, and Y. Shai. 1996. Reversible surface aggregation in pore formation by pardaxin. *Biophys. J.* 70:2502–2512.

Rapaport, D., and Y. Shai. 1991. Interaction of fluorescently labeled pardaxin and its analogues with lipid bilayers. *J. Biol. Chem.* 266: 23769–23775.

Rapaport, D., and Y. Shai. 1992. Aggregation and organization of pardaxin in phospholipid membranes: a fluorescence energy transfer study. *J. Biol. Chem.* 267:6502–6509.

Shai, Y. 1994. Pardaxin: channel formation by a shark repellant peptide from fish. *Toxicology.* 87:109–129.

Shai, Y., D. Bach, and A. Yanovsky. 1990. Channel formation properties of synthetic pardaxin and analogues. *J. Biol. Chem.* 265:20202–20209.

Shai, Y., J. Fox, C. Caratsch, Y. L. Shih, C. Edwards, and P. Lazarovici. 1988. Sequencing and synthesis of pardaxin, a polypeptide from the Red Sea Moses sole with ionophore activity. *FEBS Lett.* 242:161–166.

Shai, Y., Y. R. Hadari, and A. Finkels. 1991. pH-dependent pore formation properties of pardaxin analogues. *J. Biol. Chem.* 266:22346–22354.

Shoji, A., T. Ozaki, T. Fujito, K. Deguchi, and I. Ando. 1987. High-Resolution ^{15}N NMR-study of solid homopolypeptides by the cross-polarization magic angle spinning method: conformation-dependent ^{15}N chemical-shifts characteristic of the α-helix and β-sheet forms. *Macromolecules.* 20:2441–2445.

Siegel, D. P. 1999. The modified stalk mechanism of lamellar/inverted phase transitions and its implications for membrane fusion. *Biophys. J.* 76:291–313.

Thayer, A. M., and S. J. Kohler. 1981. Phosphorus-31 nuclear magnetic resonance spectra characteristic of hexagonal and isotropic phospholipid phases generated from phosphatidylethanolamine in the bilayer phase. *Biochemistry.* 20:6831–6834.

Thompson, S. A., K. Tachibana, K. Nakanishi, and I. Kubota. 1986. Melittin-like peptides from the shark-repelling defense secretion of the sole *Pardachirus-pavoninus*. *Science.* 233:341–343.

Tytler, E. M., G. M. Anantharamaiah, D. E. Walker, V. K. Mishra, M. N. Palgunachari, and J. P. Segrest. 1995. Molecular basis for prokaryotic specificity of magainin-induced lysis. *Biochemistry.* 34:4393–401.

Washburn, E. W., C. J. West, and C. Hull. 1926. International Critical Tables of Numerical Data, Physics, Chemistry, and Technology. McGraw-Hill, New York.

Zagorski, M. G., D. G. Norman, C. J. Barrow, T. Iwashita, K. Tachibana, and D. J. Patel. 1991. Solution structure of pardaxin P-2. *Biochemistry.* 30:8009–8017.